

Intravoxel incoherent motion MRI for the initial characterization of non-fatty non-vascular soft tissue tumors

P.A. Gondim Teixeira, L. Simon, F. Sirveaux, B. Marie, M. Louis, G. Hossu, A. Blum

▶ **To cite this version:**

P.A. Gondim Teixeira, L. Simon, F. Sirveaux, B. Marie, M. Louis, et al.. Intravoxel incoherent motion MRI for the initial characterization of non-fatty non-vascular soft tissue tumors. Diagnostic and Interventional Imaging, 2020, 101 (4), pp.245-255. 10.1016/j.diii.2019.11.003 . hal-03240958

HAL Id: hal-03240958
https://hal.univ-lorraine.fr/hal-03240958

Submitted on 22 Aug 2022

HAL is a multi-disciplinary open access archive for the deposit and dissemination of scientific research documents, whether they are published or not. The documents may come from teaching and research institutions in France or abroad, or from public or private research centers.

L'archive ouverte pluridisciplinaire **HAL**, est destinée au dépôt et à la diffusion de documents scientifiques de niveau recherche, publiés ou non, émanant des établissements d'enseignement et de recherche français ou étrangers, des laboratoires publics ou privés.



Distributed under a Creative Commons Attribution - NonCommercial 4.0 International License

Version of Record: https://www.sciencedirect.com/science/article/pii/S2211568419302578
Manuscript_7055fdf7fcd569eba27959cc0d61869f

Intravoxel incoherent motion MRI for the initial characterization of non-fatty non-vascular soft tissue tumors

Short title:

IVIM for characterization of soft tissue tumors

Pedro Augusto Gondim Teixeira[1*] , Laureline Simon[1] , François Sirveaux[2] , Béatrice Marie[3] , Matthias Louis[1] , Gabriela Hossu[4] , Alain Blum[1]

1- Guilloz Imaging Department, Central Hospital, University Hospital of Nancy, 54035 Nancy cedex, France.

2- Emile Gallé Surgical Center, 54000 Nancy, France.

3- Pathology Department, Central Hospital, University Hospital of Nancy, 54035 Nancy cedex, France

4- Lorraine University, IADI laboratory, UMR S 947, 54511 Vandœuvre-lès-Nancy, France

*Corresponding author: ped_gt@hotmail.com

Département d'imagerie Guilloz, Hôpital Central,29 avenue du Maréchal de Lattre de Tassigny, 54035 Nancy cedex, France.

© 2019 published by Elsevier. This manuscript is made available under the CC BY NC user license
https://creativecommons.org/licenses/by-nc/4.0/

Abstract

PURPOSE. To compare the capabilities of intravoxel incoherent motion (IVIM) to those of monoexponential diffusion-weighted imaging for differentiating benign from malignant non-vascular, non-fatty soft tissue tumors (NVSFSTT).

MATERIAL AND METHODS. A total of 64 patients with 64 histologically confirmed soft-tissue tumors were retrospectively included. There were 23 men and 41 women with a mean age of 52 ± 17 (SD) (range: 18-92 years). IVIM parameters, including molecular diffusion restriction coefficient (ADC_{true}), perfusion fraction, and tissue perfusion related coefficient were compared to mean monoexponential ADC (ADC_{std}) values. Two readers calculated all parameters, which were compared to histopathological findings that were used as standard of reference.

RESULTS. The overall performance of ADC_{true} and ADC_{std} was similar for the benign-malignant differentiation of NFNVSTT with accuracies ranging from 73% to 75% for both readers (P=0.3). Interobserver reproducibility was considered excellent for both ADC_{std} and all IVIM parameters (ICC = 0.81-0.96). When myxoid tumors were excluded from morphological analysis, an increase in sensitivity of 16-21% of ADC_{true} was observed, with no changes in specificity values. The use of perfusion related IVIM parameters in association with ADC_{true} did not improve tumor characterization.

CONCLUSION. The use of IVIM parameters does not improve the characterization of NVNFSTT by comparison with conventional monoexponential ADC calculation.

Keywords: Intravoxel incoherent motion (IVIM); Diffusion Magnetic Resonance Imaging; Soft Tissue Neoplasms; Comparative study.

Abbreviation

NVNFSTT = Non-vascular non-fatty soft tissue tumors

DWI = Diffusion-weighted imaging

IVIM = Intravoxel incoherent motion

ADC = Apparent diffusion coefficient

ADC_{avg} = Average ADC values

ADC_{std} = Mean ADC values calculated with a monoexponential model

ADC_{true} = Molecular diffusion restriction coefficient

D* = Tissue perfusion related coefficient

f = Perfusion fraction

ROI = Region-of-interest

FSE = Fast spin-echo

NEX = Number of excitations

FOV = Field-of-view

ICC = Intraclass correlation coefficient

Introduction

Soft tissue tumors refer to a histologically heterogeneous group of tumors for which the differentiation between benign and malignant ones is paramount for the optimization of patient management [1,2]. Pseudo tumors excluded, benign and malignant non-vascular non-fatty soft tissue tumors (NVNFSTT) are particularly challenging to differentiate since these tumors may present similar characteristics on magnetic resonance imaging (MRI). Diffusion-weighted imaging (DWI) with apparent diffusion coefficient (ADC) analysis can provide an additional quantitative criterion for soft tissue tumor characterization. However the performance of standard DWI for NVNFSTT benign-malignant differentiation is still insufficient to change patient management because of sensitivities and specificities ranging between 75-94% and 59-88% respectively) [3–6].

Standard ADC calculation in DWI is derived from a monoexponential model, which does not allow an accurate separation between intra-vascular diffusion (perfusion) and extra-

vascular extra-cellular diffusion (true tissue diffusion). The vascularity of NVNFSTT is highly variable, and previous studies showed that perfusion parameters have limited performances in the differentiation between benign and malignant tumors [7]. This perfusion heterogeneity could act as a confounding factor in monoexponential DWI particularly at low b values (<200 s/mm^2) with micro-capillary water displacement acting as a pseudo-diffusion effect [8,9]. Intravoxel incoherent motion (IVIM) MRI uses a bi-exponential approach to DWI data allowing the separation between the influence intravascular diffusion (e.g. tissue perfusion) and tissue diffusion. This technique allows quantifying microcapillary perfusion (low b values < 200 s/mm^2) and extra-vascular extra-cellular tissue diffusivity (higher b values > 200 s/mm^2) and could help overcome this difficulty potentially improving the performance of DWI for the characterization of NVNFSTT [8,10–18]. By comparison with monoexponential DWI, IVIM presents greater sensitivity and specificity for the characterization of breast tumors [12]. The perfusion fraction yielded by IVIM analysis also aided in the distinction between low- and high-grade gliomas [14]. Additional studies also suggested a benefit in using IVIM for the evaluation of other types of malignancy in the kidney, liver and pancreas [19–21]. By providing more accurate evaluation of tissue diffusivity associated with perfusion data, we hypothesized that IVIM could improve the characterization of NVNFSTT by comparison with monoexponential DWI.

IVIM MRI is based on a bi-exponential approach to signal analysis with multiple b-values (five to 16) requiring a specific acquisition sequence, which is less available and more time consuming than that used for monoexponential DWI. Most importantly, the calculation of IVIM parameters requires dedicated software, which is not always available in vendor clinical workstations.

The purpose of this study was to compare the capabilities of intravoxel incoherent motion (IVIM) to those of monoexponential DWI for differentiating benign from malignant NVSFSTT.

Material and methods

Patients

From September 2014 to December 2016, 131 patients with suspected soft-tissue tumors were consecutively included in a prospective study for the evaluation of noninvasive tumor characterization methods using MRI. This study was approved by the institutional ethics

committee; all patients were major and signed an informed consent form. Patients had been referred for initial tumor characterization and local staging and had no prior surgery or biopsies at the time of imaging. Pregnancy and MR contra-indications were general exclusion criteria for this study. Histologic analysis based on core biopsy specimens was performed in our institution after MR imaging.

Three patients were excluded because no histologic confirmation was available. Eight patients were excluded because the multi-b value diffusion-weighted sequence was not performed or was not available. Six patients were excluded because of significant artifacts on DWI (anatomic distortion on EPI sequences on the extremities and motion artifacts in non-compliant patients). Thirteen patients with cystic pseudo-tumors and 19 with fatty tumors were excluded because water diffusion in cystic tumors or in tumors containing fat differs considerably from that non-fatty tumors [22] . Finally, seventeen patients with vascular tumors were excluded as ADC is influenced by tumor perfusion and by the amount of intratumor fat. Cystic, fatty, and vascular tumors were identified based on MRI findings. Cystic tumors were characterized by fluid signal intensity on T1 and T2-weighted images without internal contrast enhancement; fatty tumors were characterized by the presence of intratumoral fat signal, hyperintense on T1-weighted images and hypointense on fat-suppressed sequences; vascular tumors were characterized by the presence of serpiginous vessel-like structures within the tumor and a vascular enhancement pattern on perfusion MRI.

Thus, the final study population was composed of 65 patients with histologically confirmed “de novo” NVNFSTT (Fig. 1). There were 23 men and 41 women with a mean age of 52 ± 17 (SD) (range: 18-92 years).

MRI examination

MRI examinations was performed at 3T (Discovery MR750W 3.0T, GE Healthcare) using dedicated coils. Acquisition parameters for conventional and diffusion-weighted sequences are presented in table 1. A gadobenate dimeglumine based contrast medium (Multihance® 20 mL, Bracco Diagnostics) was used. Total DWI scan time varied from 180s to 300s depending on the number of slices necessary to cover the tumors studied.

Image analysis

Image post-processing was performed with the OleaSphere® V2.3 workstation (Olea Medical SA, La Ciotat, France) with the IVIM application module. Two methods were used to analyze

DWI data: Monoexponential analysis was performed using only three of the acquired b values (60, 500, 900 s/mm^2) to calculate the apparent diffusion coefficient (ADC_{std}). Standard ADC estimation is very sensitive to noise and sampling. Thus, Bayesian probability theory was used in order to estimate this parameter better. A Bi-exponential Bayesian model was also used to calculate the molecular diffusion restriction coefficient (ADC_{true}), perfusion fraction (f) and tissue perfusion related coefficient (D*). After post-processing four color functional maps were automatically generated by the software (ADC_{std}, ADC_{true}, f, and D*).

The images were analyzed by two radiologists with four and ten years of clinical experience with MRI. Functional diffusion maps were correlated with axial T2-weighted fat-saturated images and contrast-enhanced T1-weighted fat-saturated images to allow identification of areas with cystic or necrotic tumors. The post-processing software allowed a side-by-side comparison between functional maps and conventional imaging series with the possibility to superimpose the color maps over conventional images with various degrees of transparency. To allow selection of a representative value, a free form ROI on the functional ADC_{std} maps was used according to the following procedure proposed by Bonarelli et al. [4,26]: in heterogeneous tumors with cystic or necrotic components (defined as areas of unenhanced tumor), a free form ROI was placed over the solid tumor portion with the lowest ADC_{std} values by the less experienced reader. In homogeneously enhancing tumors, a free form ROI covering the largest tumor surface possible was drawn (Fig.2). ROI size was case dependent. All slices depicting tumor were analyzed.

Tumors with fluid-like high signal on T2-weighted sequences, low signal on T1-weighted sequences, and a low heterogeneous enhancement were considered as myxoid imaging characteristics [23–25].

Statistical analysis

The results of the histopathological analysis were used as the standard of reference. Quantitative data are presented as mean ± standard deviation (range). A paired student's t-test was used to evaluate the differences between ADC_{std} and ADC_{true} values. The intraclass correlation coefficient (ICC) was used to evaluate the impact of ROI positioning on the parameters studied. The Kruskal-Wallis and the Spearman's rank correlation test were used to verify a potential association between ADC values both ADC_{std} and ADC_{true} values with tumor location and size respectively. For all analyses, $P < 0.05$ was considered as the threshold for statistical significance. Univariate and multivariate receiver-operating

characteristic (ROC) curve analysis were performed to determine the optimal cutoff for differentiation between benign and malignant tumors for each and for combinations of the parameters studied. Sensitivity, specificity, accuracy and their 95% confidence interval as well as the areas-under-the-curve (AUC) were calculated. The latter have been calculated by a stratified bootstrap algorithm with 2000 replicates (pROC package in R software). The McNemar test was used to evaluate the statistical significance of the sensitivity and specificity for benign-malignant differentiation with the different parameters studied. Statistical analysis was performed by a statistical expert (H.G). with 10 years of practice using statistics software (R, version 3.6.0, R Project for Statistical Computing).

Results

Histologically, 35 of the tumors evaluated were benign, and 29 were malignant. Tumor histological subtypes are presented in Table 2. The mean tumor diameter was 46 ± 29 (SD) mm (range: 9-160 mm) for all tumors, 60 ±33 (SD) mm (range: 13-160 mm) for malignant tumor and 34 ± 16 (SD) mm (range: 9-78 mm) for benign tumors. Regarding the anatomical distribution, there were 12 tumors in the upper limb, 37 in the lower limb and 15 in the body. The mean ROI sizes in the studied tumors were 634 ± 632 (SD) mm^2 (range: 17-2586 mm^2), ROI sizes were larger for malignant tumors compared to benign tumors with mean ROI sizes of 1037 ± 694 (SD) mm2 (range: 144-2131 mm2) and 299 ± 300 (SD) mm^2 (range: 17-2585 mm^2)respectively ($P < 0.0001$). There was no significant variation in ADC_{std} and ADC_{true} values with respect to tumor diameter and location ($P > 0.18$).

When all tumors were considered (benign and malignant), there was a statistically significant difference between ADC_{std} and ADC_{true} values, the former presenting higher values than the latter ($P < 0.0001$ for both readers). The ADCtrue and ADCstd values were significantly lower in malignant tumors (Fig.3) compared to benign ones ($P < 0.003$ for both readers). Conversely, D* values were significantly greater for malignant tumors than benign tumors (P=0.01 and 0.05 for Readers 1 and 2, respectively). Interobserver reproducibility was considered excellent for ADC_{std} values (ICC = 0.96), and on IVIM parameters (ICC: 0.81-0.96) obtained with all tumor ROIs. The mean values of the parameters evaluated and the respective ICC values in each of the evaluated sub-groups are presented in table 3.

The overall performance of ADC_{true} and ADC_{std} was similar for the benign-malignant differentiation of NFNVSTT with accuracies of 73 % and 75 % for Readers 1 and 2, respectively (AUC = 0.74-0.73 and 0.74-0.75 for ADC_{std} and ADC_{true}, respectively) ($P = 0.3$).

The specificity of ADC_{true} values was greater than that of ADC_{std} values for both readers (91 % vs. 83-86 %) but these differences were not statistically significant ($P > 0.47$). Sensitivity values were greater with ADC_{std} (62-66%) compared to ADC_{true} (52%) for both readers ($P < 0.001$). D* value analysis showed an accuracy of 67 % and 72 % for benign-malignant differentiation for readers 1 and 2, respectively, while f values yielded lower accuracies (52 % and 53 % for readers 1 and 2). When ADC_{true}, D* and f values were analyzed in combination, multivariate ROC analysis with did not show any improvement in diagnostic performance with values with respect to ADC_{std} alone (accuracies varying from 73% to 75% for both readers). The best AUC was found with the combination of ADC_{true} and f analysis (0.75). The full performance analysis of all parameters evaluated and the respective cutoff values are provided in Table 4. A comparison of the ROC curves of the parameters evaluated is presented in Figure 4.

When tumors for which ADC_{true} values were falsely positive and falsely negative were analyzed, the perfusion related IVIM parameters (f and D*) did not improve tumor characterization. There was a high coefficient of variation of f values (54% for both readers) and D* values (88.5% for Reader 1 and 91% for Reader 2) among false positive and false negative tumors. There were three and four false positive findings for Readers 1 and 2, respectively, with ADC_{true} analysis, two granular cell tumors, and a giant cell tumor. The additional tumor for Reader 2 was a desmoid fibromatosis. With ADC_{std} analysis, the histology of false positives tumors also included another desmoid fibromatosis, a myofibroblastic tumor, and a schwannoma. With ADC_{true} analysis, there were 12 false-negative tumors for both readers. Among these 12 tumors, 7/12 (58%) had a myxoid component on histologic analysis.

All 12 myxoid tumors evaluated (both malignant and benign) presented an ADC_{true} value higher than the cutoff value of 96 $\times 10^{-3}$ mm^2/s (Fig.5). The mean ADC_{true} values in these tumors were 245 ± 39 (SD) × 10^{-3} mm^2/s (range: 193-282 × 10^{-3} mm^2/s) in benign and 152 ± 10^{-3} mm^2/s (range: 77-240 × 10^{-3} mm^2/s) in malignant tumors for reader 1 and 240 ± 33 (SD) $\times 10^{-3}$ mm^2/s (range: 186-274 × 10^{-3} mm^2/s) and 148 ± 48 (SD) 10^{-3} mm^2/s (range: 109-229 × 10^{-3} mm^2/s) for reader 2 respectively. Among these tumors, ten showed myxoid imaging characteristics on conventional MRI (four myxomas, five myxoid sarcomas, and one neurofibroma). When the tumors with myxoid features on conventional MRI were excluded, the ADC_{true} accuracy increased from 73% to 78-83%. There was an improvement in sensitivity from 52% to 68-73% with a similar specificity ($P > 0.7$). The ADC_{std} values

showed a similar variation after the exclusion of myxoid tumors. Mean, and standard deviation of all parameters evaluated in tumors without myxoid imaging characteristics as well as the diagnostic performance of these parameters are reported in Table 5.

Discussion

Despite the statistically significant differences between ADC_{std} and ADC_{true} in the tumors evaluated and the theoretical advantages of bi-exponential analysis of DWI data, there were no significant differences in the diagnostic performance of these two parameters for benign-malignant differentiation of NVNFSTT. The best sensitivity was reached with ADC_{std} (62-66%) and the best specificity with ADC_{true} (91%). There were no noticeable differences in the numbers of false-positive and false-negative tumors found with ADC_{std} and ADC_{true}. The reproducibility of IVIM parameters and ADC_{std} were both considered excellent (ICC = 0.81-0.96). Lim et al. reported a similar performance between standard and true ADC values in musculoskeletal tumors[27]. These authors, however, did not access the added value of IVIM directly to monoexponential diffusion analysis. Moreover, the use of perfusion related IVIM parameters in association with ADC_{true} did not improve tumor characterization, with a high variation in D* and f values among ADC_{true} false positive and false negative tumors. These results indicate that factors other than tumor perfusion, such as tissue extra-cellular architecture and collagen content may as confounding factors for NVNFSTT characterization with DWI [4]. Thus, until other technical solutions are available to overcome these difficulties, the use of monoexponential DWI (less time consuming and more widely available than IVIM) should be used for soft tissue tumor characterization.

In our study, perfusion related IVIM parameters showed an average performance for the characterization of NVNFSTT with D* yielding the best results with a sensitivity of 62% and 80% and specificity values. This average performance is similar to previously published reports on contrast-enhanced dynamic MRI for soft tissue tumor characterization and is probably related to the multiple histologic subtypes of these tumors which translated to an important variability in tumor vascularity[1,7,28]. Marzi et al. did not show a significant relationship between IVIM parameters and any dynamic contrast-enhanced MRI parameters [29]. These differences can be related to a possible extravascular diffusion of contrast medium in dynamic contrast-enhanced MRI, whereas the IVIM perfusion parameters are thought to be more representative of the intravascular perfusion. Similarly to contrast-enhanced dynamic MRI, IVIM related perfusion could be more useful in for the detection of tumor recurrence or

for the evaluation of adjuvant treatment response, but further studies are needed to investigate this matter [30-32].

Compared to monoexponential analysis, the bi-exponential analysis did not improve the performance of ADC for the characterization of myxoid tumors, which represented more than half of the false negative tumors encountered with ADC_{true} analysis. Similar to previous literature reports with monoexponential ADC values, ADC_{true} analysis did not allow differentiation between the benign and malignant myxoid tumors of the studied population [25]. Interestingly, ten out of the 12 (83%) tumors with myxoid components identified histologically presented a myxoid aspect on conventional MRI. Moreover, when tumors with myxoid features were excluded from the analysis, a 16-21% increase in the sensitivity of ADC_{true} analysis was noted with a minimal decrease in specificity. These findings suggest ADC analysis should not be performed in tumors with myxoid features on conventional MRI [23,25,26].

The main limitation of this study is the small sample size considering the variability in the histological aspects of NVNFSTT. We chose to evaluate a histologically heterogeneous tumor group, which probably influenced the diagnostic performance of our parameters because this represents daily clinical practice in oncological imaging centers and any imaging technique that improves tumor characterization should be useful in this context. This, however, did not influence the main objective of this study, which was to compare the diagnostic performance of bi- and monoexponential derived DWI parameters. DWI data were not analyzed in association with conventional morphologic imaging, which is the standard clinical practice because this was a preliminary study with a relatively small number of patients, aimed at assessing the diagnostic accuracy of IVIM in tumor characterization. Further studies are needed to evaluate the benefit of a combined approach including conventional morphologic analysis and DWI, particularly monoexponential ADC for NVNFSTT characterization. Extremity tumors (hand fingers and forefoot) were prone to distortion artifact with EPI based sequences. Other pulse sequences for DWI acquisition are likely necessary to evaluate these tumors.

In conclusion, the use of IVIM parameters did not improve the characterization of NVNFSTT compared to conventional monoexponential ADC calculation. As DWI remains a valid tool for the characterization of soft tissue tumors in a multiparametric approach combined with morphologic tumor analysis on conventional sequences, these results support the use of standard monoexponential DWI, which has a more straightforward acquisition

protocol with fewer b values, is less time consuming and more widely available than IVIM MRI.

Conflicts of interest

The authors have no conflicts of interest to disclose.

Funding Sources

This article did not receive a specific funding.

References

[1] Jo VY, Fletcher CDM. WHO classification of soft tissue tumors: an update based on the 2013 (4th) edition. Pathology 2014;46:95–104.

[2] Wu JS, Hochman MG. Soft-tissue tumors and tumorlike lesions: a systematic imaging approach. Radiology 2009;253:297–316.

[3] Razek A, Nada N, Ghaniem M, Elkhamary S. Assessment of soft tissue tumours of the extremities with diffusion echoplanar MR imaging. Radiol Med 2012;117:96–101.

[4] Teixeira PAG, Gay F, Chen B, Zins M, Sirveaux F, Felblinger J, et al. Diffusion-weighted magnetic resonance imaging for the initial characterization of non-fatty soft tissue tumors: correlation between T2 signal intensity and ADC values. Skeletal Radiol 2016;45:263–71.

[5] Teixeira PAG, Gervaise A, Louis M, Raymond A, Formery A-, Lecocq S, et al. Musculoskeletal wide-detector CT kinematic evaluation: from motion to image. Semin Musculoskelet Radiol 2015;19:456–62.

[6] Subhawong TK, Jacobs MA, Fayad LM. Diffusion-weighted MR imaging for characterizing musculoskeletal lesions. Radiographics 2014;34:1163–77.

[7] Leplat C, Hossu G, Chen B, De Verbizier J, Beaumont M, Blum A, et al. Contrast-enhanced 3-T Perfusion MRI with quantitative analysis for the characterization of musculoskeletal tumors: is it worth the trouble? AJR Am J Roentgenol 2018;211:1092–8.

[8] Le Bihan D, Turner R, MacFall JR. Effects of intravoxel incoherent motions (IVIM) in steady-state free precession (SSFP) imaging: application to molecular diffusion imaging. Magn Reson Med 1989;10:324–37.

[9] Le Bihan D, Breton E, Lallemand D, Aubin ML, Vignaud J, Laval-Jeantet M. Separation of diffusion and perfusion in intravoxel incoherent motion MR imaging. Radiology 1988;168:497–505.

[10] Becker AS, Perucho JA, Wurnig MC, Boss A, Ghafoor S, Khong PL, et al. Assessment of cervical cancer with a parameter-free intravoxel incoherent motion imaging algorithm. Korean J Radiol 2017;18:510–8.

[11] Cui Y, Dyvorne H, Besa C, Cooper N, Taouli B. IVIM Diffusion-weighted Imaging of the Liver at 3.0T: Comparison with 1.5T. Eur J Radiol Open 2015;2:123–8.

[12] Liu C, Liang C, Liu Z, Zhang S, Huang B. Intravoxel incoherent motion (IVIM) in evaluation of breast lesions: comparison with conventional DWI. Eur J Radiol 2013;82:e782–9.

[13] Luciani A, Vignaud A, Cavet M, Nhieu JTV, Mallat A, Ruel L, et al. Liver cirrhosis: intravoxel incoherent motion MR imaging--pilot study. Radiology 2008;249:891–9.

[14] Federau C, Meuli R, O'Brien K, Maeder P, Hagmann P. Perfusion measurement in brain gliomas with intravoxel incoherent motion MRI. AJNR Am J Neuroradiol 2014;35:256–62.

[15] Gaeta M, Benedetto C, Minutoli F, D'Angelo T, Amato E, Mazziotti S, et al. Use of diffusion-weighted, intravoxel incoherent motion, and dynamic contrast-enhanced MR imaging in the assessment of response to radiotherapy of lytic bone metastases from breast cancer. Acad Radiol 2014;21:1286–93.

[16] Qi LP, Yan WP, Chen KN, Zhong Z, Li XT, Cai K, et al. Discrimination of malignant versus benign mediastinal lymph nodes using diffusion MRI with an IVIM model. Eur Radiol 2018; 28:1301-9.

[17] Nguyen A, Ledoux J-B, Omoumi P, Becce F, Forget J, Federau C. Selective microvascular muscle perfusion imaging in the shoulder with intravoxel incoherent motion (IVIM). Magn Reson Imaging 2017;35:91–7.

[18] van Rijswijk CSP, Kunz P, Hogendoorn PCW, Taminiau AHM, Doornbos J, Bloem JL. Diffusion-weighted MRI in the characterization of soft-tissue tumors. J Magn Reson Imaging 2002;15:302–7.

[19] Rheinheimer S, Stieltjes B, Schneider F, Simon D, Pahernik S, Kauczor HU, et al. Investigation of renal lesions by diffusion-weighted magnetic resonance imaging applying intravoxel incoherent motion-derived parameters--initial experience. Eur J Radiol 2012;81:e310–6.

[20] Yamada I, Aung W, Himeno Y, Nakagawa T, Shibuya H. Diffusion coefficients in abdominal organs and hepatic lesions: evaluation with intravoxel incoherent motion echo-planar MR imaging. Radiology 1999;210:617–23.

[21] Kang KM, Lee JM, Yoon JH, Kiefer B, Han JK, Choi BI. Intravoxel incoherent motion diffusion-weighted MR imaging for characterization of focal pancreatic lesions. Radiology 2014;270:444–53.

[22] Subhawong TK, Durand DJ, Thawait GK, Jacobs MA, Fayad LM. Characterization of soft tissue masses: can quantitative diffusion weighted imaging reliably distinguish cysts from solid masses? Skeletal Radiol 2013;42:1583–92.

[23] Petscavage-Thomas JM, Walker EA, Logie CI, Clarke LE, Duryea DM, Murphey MD. Soft-tissue myxomatous lesions: review of salient imaging features with pathologic comparison. Radiographics 2014;34:964–80.

[24] Maeda M, Matsumine A, Kato H, Kusuzaki K, Maier SE, Uchida A, et al. Soft-tissue tumors evaluated by line-scan diffusion-weighted imaging: influence of myxoid matrix on the apparent diffusion coefficient. J Magn Reson Imaging 2007;25:1199–204.

[25] Kim HS, Kim J-H, Yoon YC, Choe BK. Tumor spatial heterogeneity in myxoid-containing soft tissue using texture analysis of diffusion-weighted MRI. PloS One 2017;12:e0181339.

[26] Bonarelli C, Teixeira PAG, Hossu G, Meyer J-B, Chen B, Gay F, et al. Impact of ROI positioning and lesion morphology on apparent diffusion coefficient analysis for the differentiation between benign and malignant nonfatty soft-tissue lesions. AJR Am J Roentgenol 2015;205:W106–13.

[27] Lim HK, Jee WH, Jung JY, Paek MY, Kim I, Jung CK, et al. Intravoxel incoherent motion diffusion-weighted MR imaging for differentiation of benign and malignant musculoskeletal tumours at 3 T. Br J Radiol 2018;91:20170636.

[28] van Rijswijk CSP, Geirnaerdt MJA, Hogendoorn PCW, Taminiau AHM, van Coevorden F, Zwinderman AH, et al. Soft-tissue tumors: value of static and dynamic gadopentetate dimeglumine-enhanced MR imaging in prediction of malignancy. Radiology 2004;233:493–502.

[29] Marzi S, Stefanetti L, Sperati F, Anelli V. Relationship between diffusion parameters derived from intravoxel incoherent motion MRI and perfusion measured by dynamic contrast-enhanced MRI of soft tissue tumors. NMR Biomed 2016;29:6–14.

[30] Teixeira PAG, Beaumont M, Gabriela H, Bailiang C, Verhaeghe J, Sirveaux F, et al. Advanced Techniques in Musculoskeletal Oncology: Perfusion, Diffusion, and Spectroscopy. Semin Musculoskelet Radiol 2015;19:463–74.

[31] Thakran S, Gupta PK, Kabra V, Saha I, Jain P, Gupta RK, Singh A. Characterization of breast lesion using T1-perfusion magnetic resonance imaging: qualitative vs. quantitative analysis. Diagn Interv Imaging 2018;99:633-42.

[32] Gondim Teixeira PA, Renaud A, Aubert S, Ben Haj Amor M, Robin YM, Cotten A, Ceugnart L. Perfusion MR imaging at 3-Tesla: can it predict tumor grade and histologic necrosis rate of musculoskeletal sarcoma? Diagn Interv Imaging 2018;99:473-81

Figures

Fig. 1 – Study flowchart shows patients and tumors selection.

Fig. 2 – Region of interest (ROI) positioning procedure according to tumor morphologic features. A and B) 65-year-old man with a high-grade sarcoma of the leg. A) T1-weighted fat-saturated gadolinium chelate-enhanced MR image in the axial plane shows homogeneous enhancement of a soft-tissue tumor. B) Apparent diffusion coefficient (ADC) standard functional map shows a free form ROI drawn over the tumor's contours to include the largest portion of the tumor possible (dashed line). C and D) 63-year-old woman with a pre-sacral mesenchymal chondrosarcoma associated with local sacrococcygeal bone invasion. C) T1-weighted fat-saturated gadolinium chelate -enhanced MR image in the axial plane shows heterogeneously enhancing tumor (arrowheads) with central areas of necrosis (arrows). D) ADC standard functional map shows free form ROI drawn to delineate the viable tumor zone with the lowest ADC possible (dashed line) while avoiding the central necrotic areas (arrows) tumor's contours.

Fig. 3 – Fifty-year-old man with Ewing sarcoma of the right thigh. A) T1-weighted fat-saturated gadolinium chelate-enhanced MR image in the axial plane shows an anterolateral homogeneously enhancing soft tissue tumor of the distal thigh (arrowheads), with associated popliteal adenopathy (arrow). B) and C) functional ADC maps obtained with monoexponential analysis (B) and bi-exponential IVIM analysis (C), both show the same tumor (arrowheads) with low ADC values indicative of malignant tumor (0.95×10^{-3} mm^2/s and 0.69×10^{-3} mm^2/s respectively).

Fig. 4 – ROC analysis of the diagnostic performance of IVIM parameters and standard apparent diffusion coefficient (ADC) datasets studied for differentiation between benign and malignant nonfatty nonvascular soft-tissue tumors individually (A) and combined (B). None the superposition of the ADC_{std} and ADC_{true} curves with similar area-under-the-curve (AUC) values (blue and orange curves respectively).

Fig. 5 – 37-year-old woman with extraskeletal myxoid chondrosarcoma of the distal left thigh. A) T2-weighted fat-saturated MR image in the axial plane shows heterogeneous intra-muscular tumor with areas of fluid-like hyperintensity (arrowheads). B) T1-weighted fat-saturated gadolinium-enhanced MR image in the axial plane shows a predominantly peripheral enhancement (arrows) and a non-enhancing central area indicative of tumor necrosis. C, D, and E) functional IVIM derived maps (molecular diffusion restriction coefficient, perfusion fraction and D* respectively) show high ADC (2.49×10^{-3} mm^2/s) and low perfusion fraction (0.11) and pseudo-diffusion coefficient (2.8×10^{-3} mm^2/s) measured in the areas delineated by the dashed free form ROI. IVIM parameters were falsely consistent with a benign tumor whereas the patient had a malignant tumor.

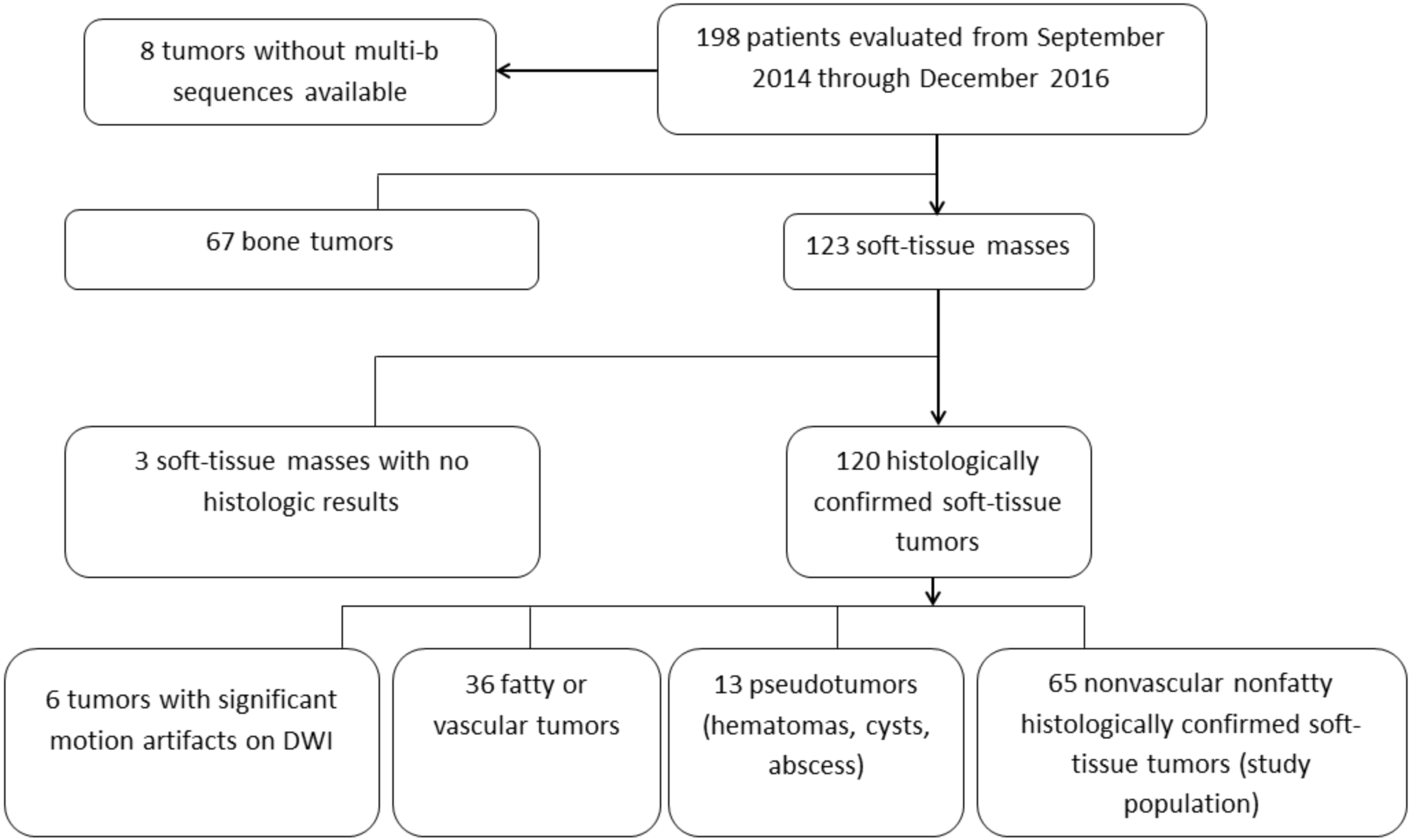
Table 1. MR imaging acquisition protocol.

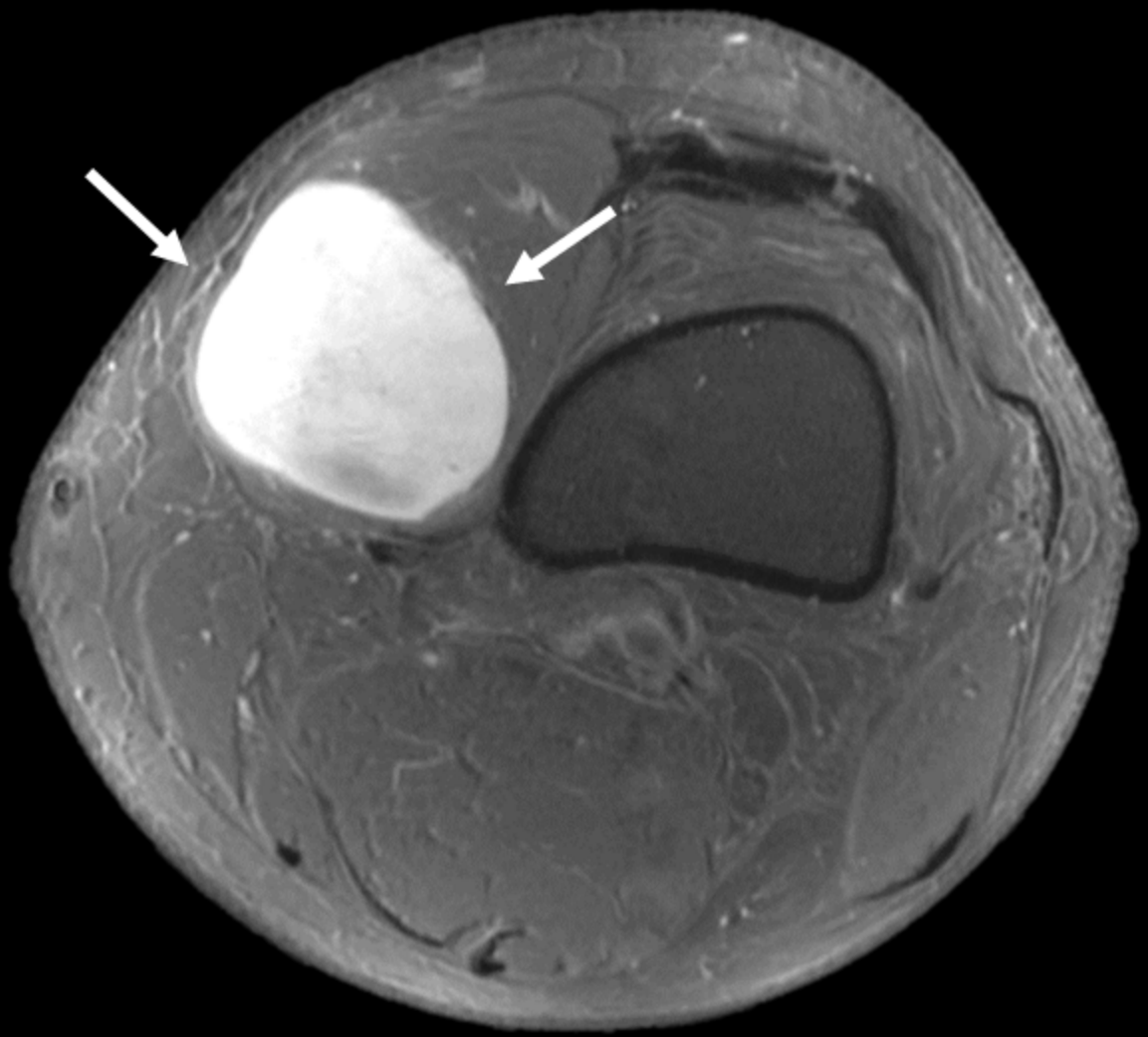
Table 2. Histologic subtypes of 65 tumors in 65 patients with soft tissue tumors

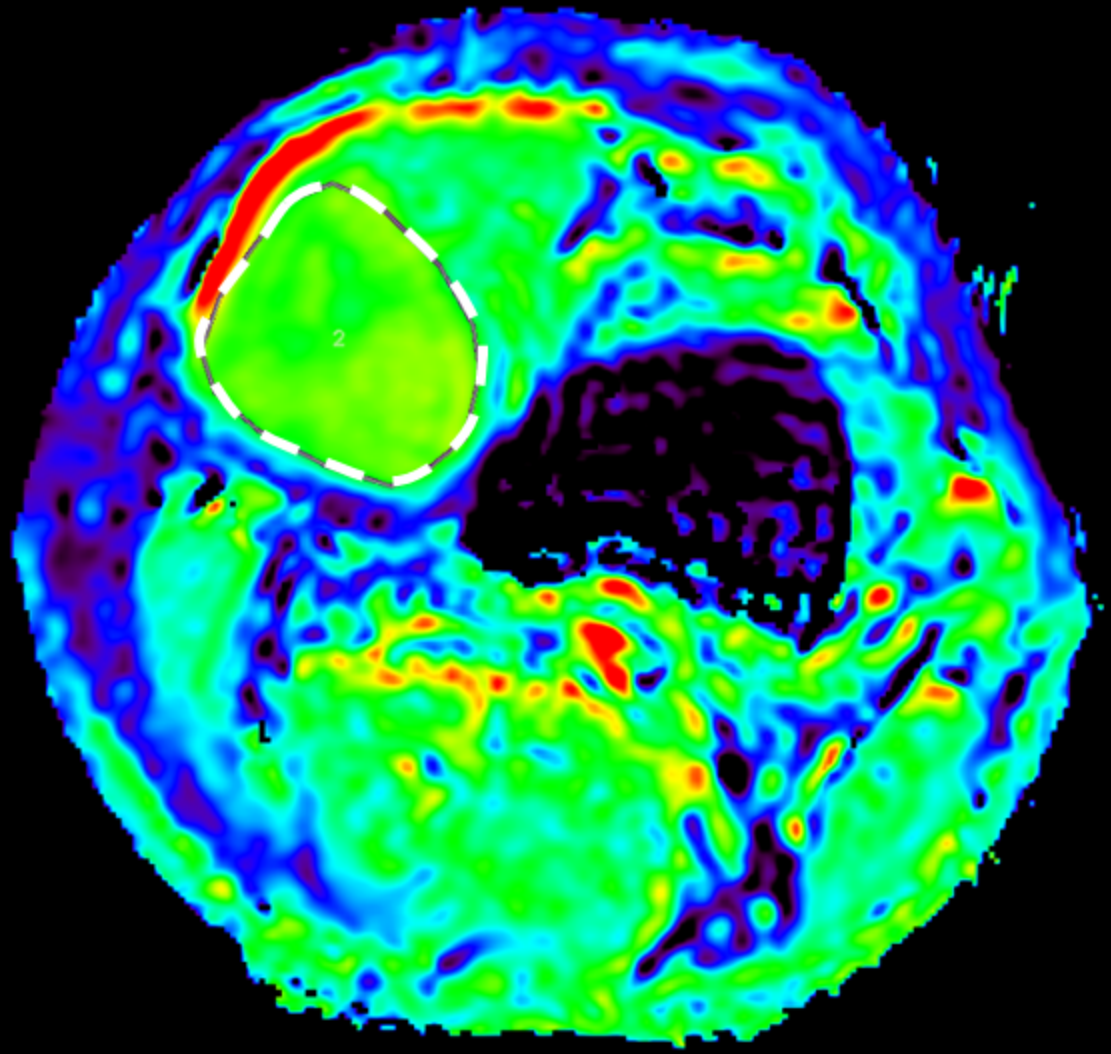
Table 3. Value distribution of the monoexponential and bi-exponential diffusion-weighted parameters evaluated in benign and malignant tumors.

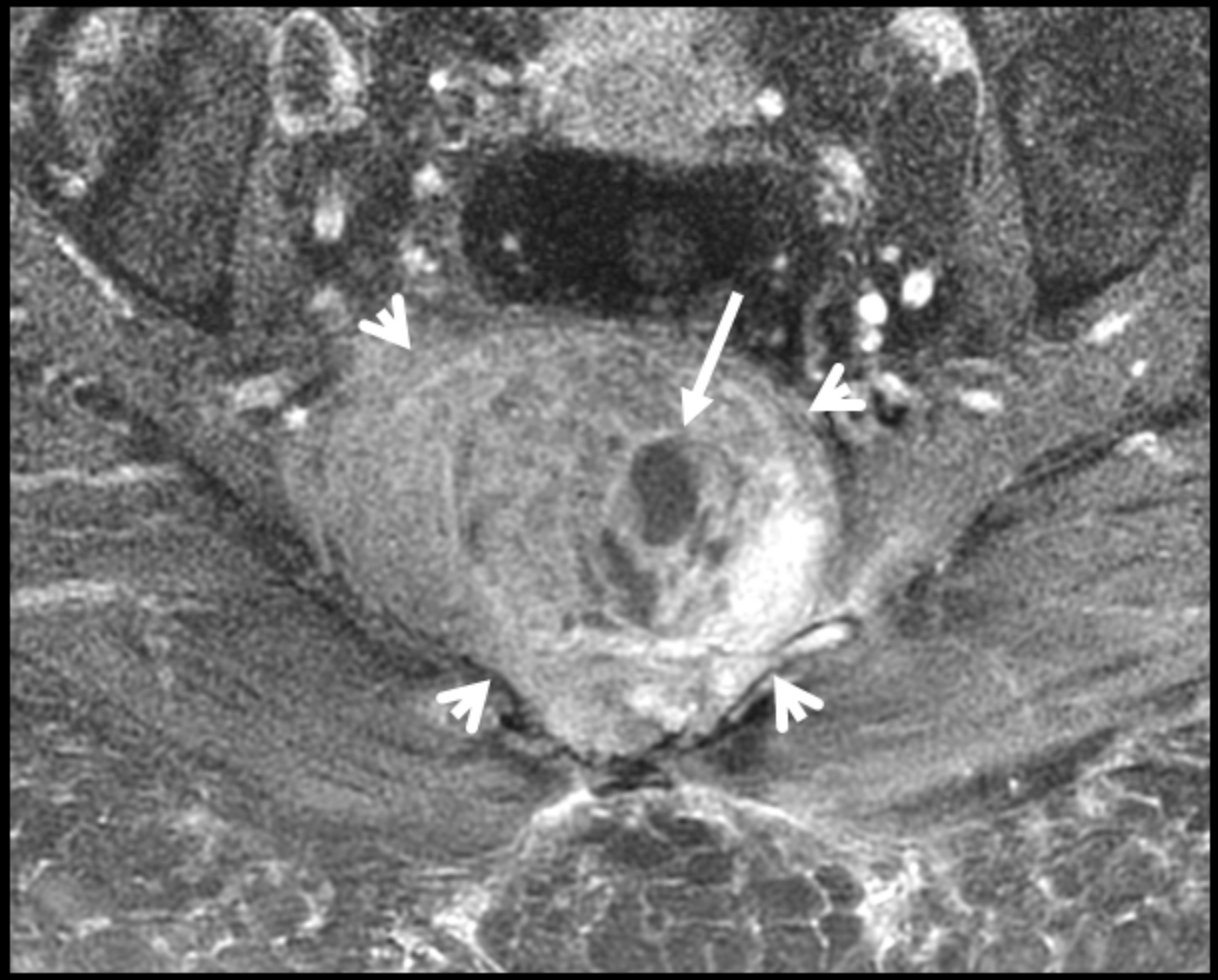
Table 4. *Diagnostic* performance of monoexponential apparent diffusion coefficient (ADC) and IVIM parameters for differentiation between benign and malignant tumors.

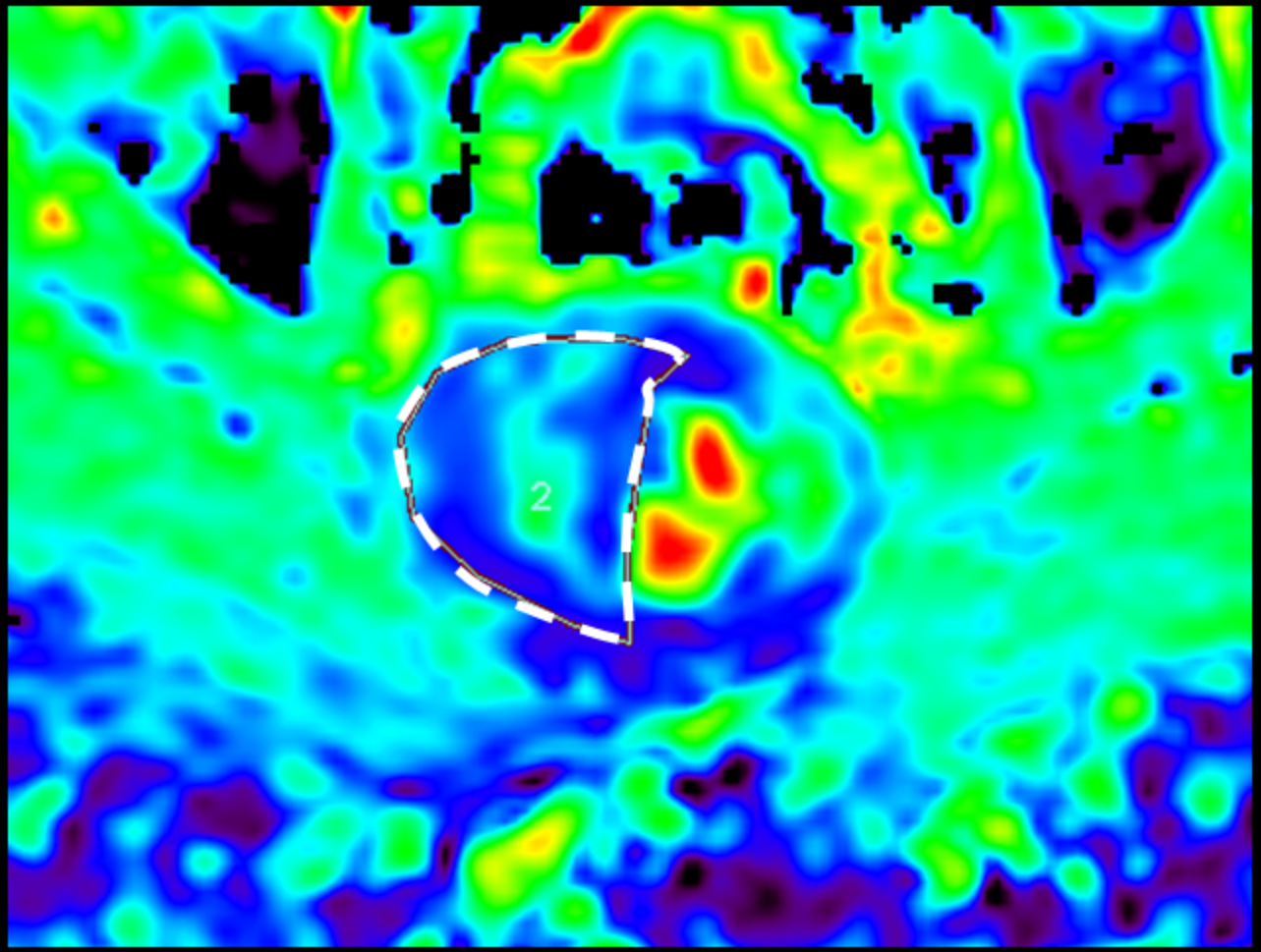
Table 5. Apparent diffusion coefficient (ADC) obtained by separating morphological subgroups with or without myxoid features on MRI.

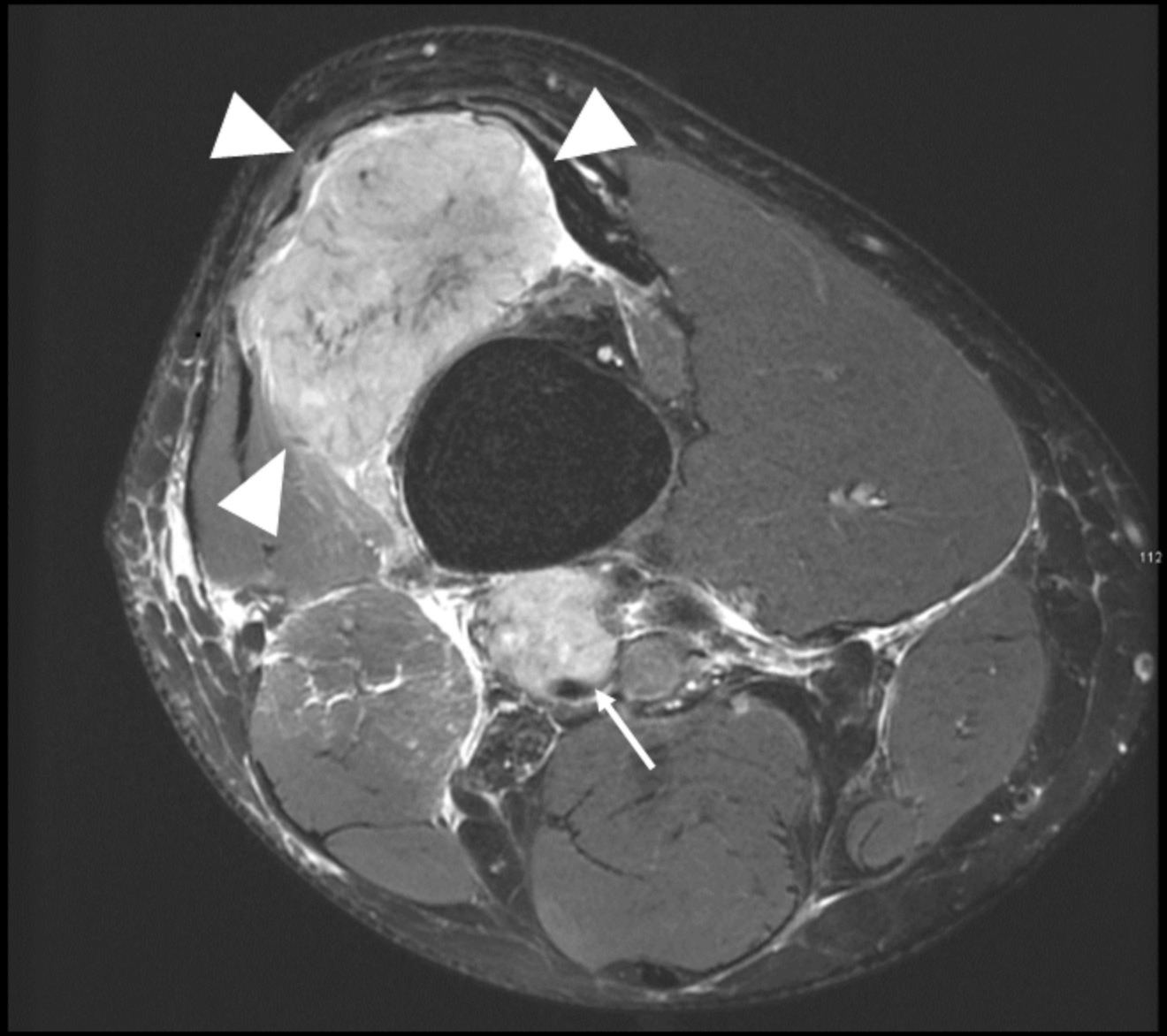

198 patients evaluated from September 2014 through December 2016
8 tumors without multi-b sequences available
67 bone tumors
123 soft-tissue masses
3 soft-tissue masses with no histologic results
120 histologically confirmed soft-tissue tumors
6 tumors with significant motion artifacts on DWI
36 fatty or vascular tumors
13 pseudotumors (hematomas, cysts, abscess)
65 nonvascular nonfatty histologically confirmed soft-tissue tumors (study population)

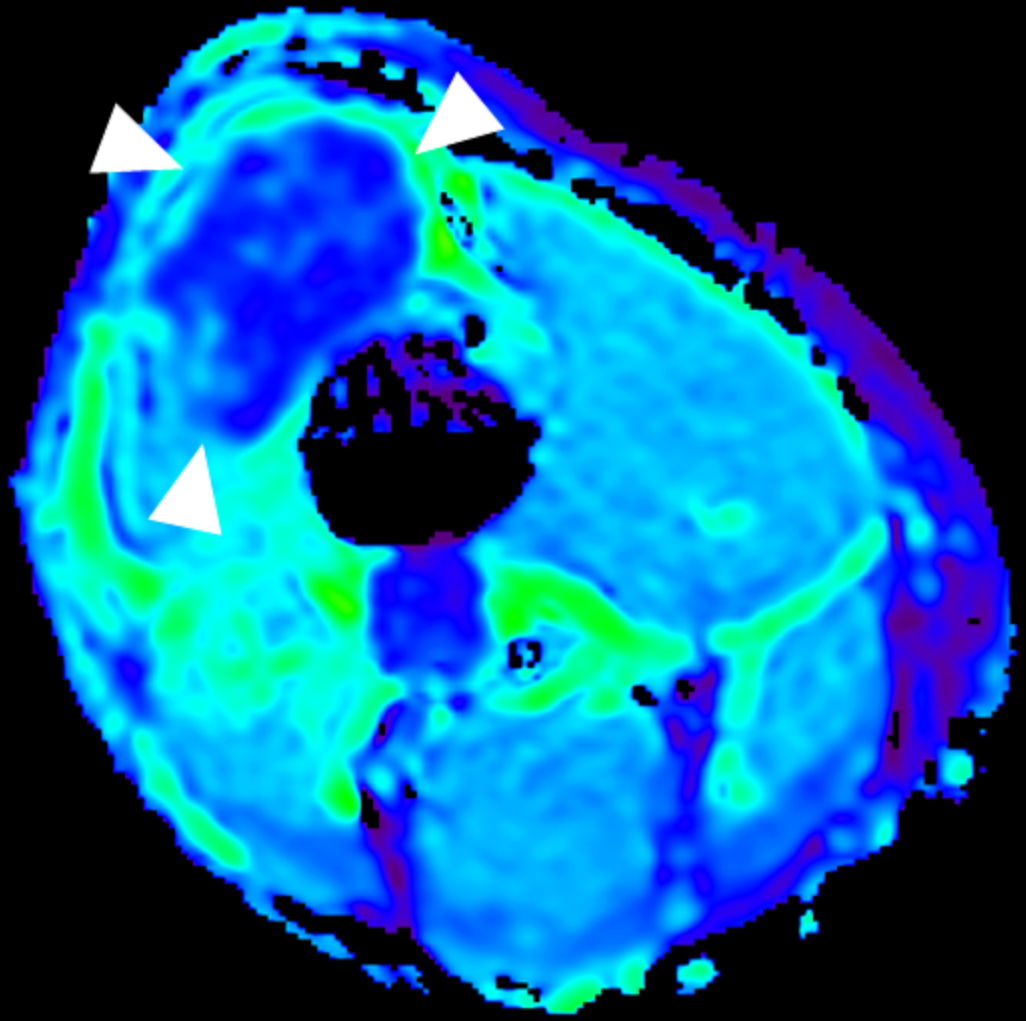


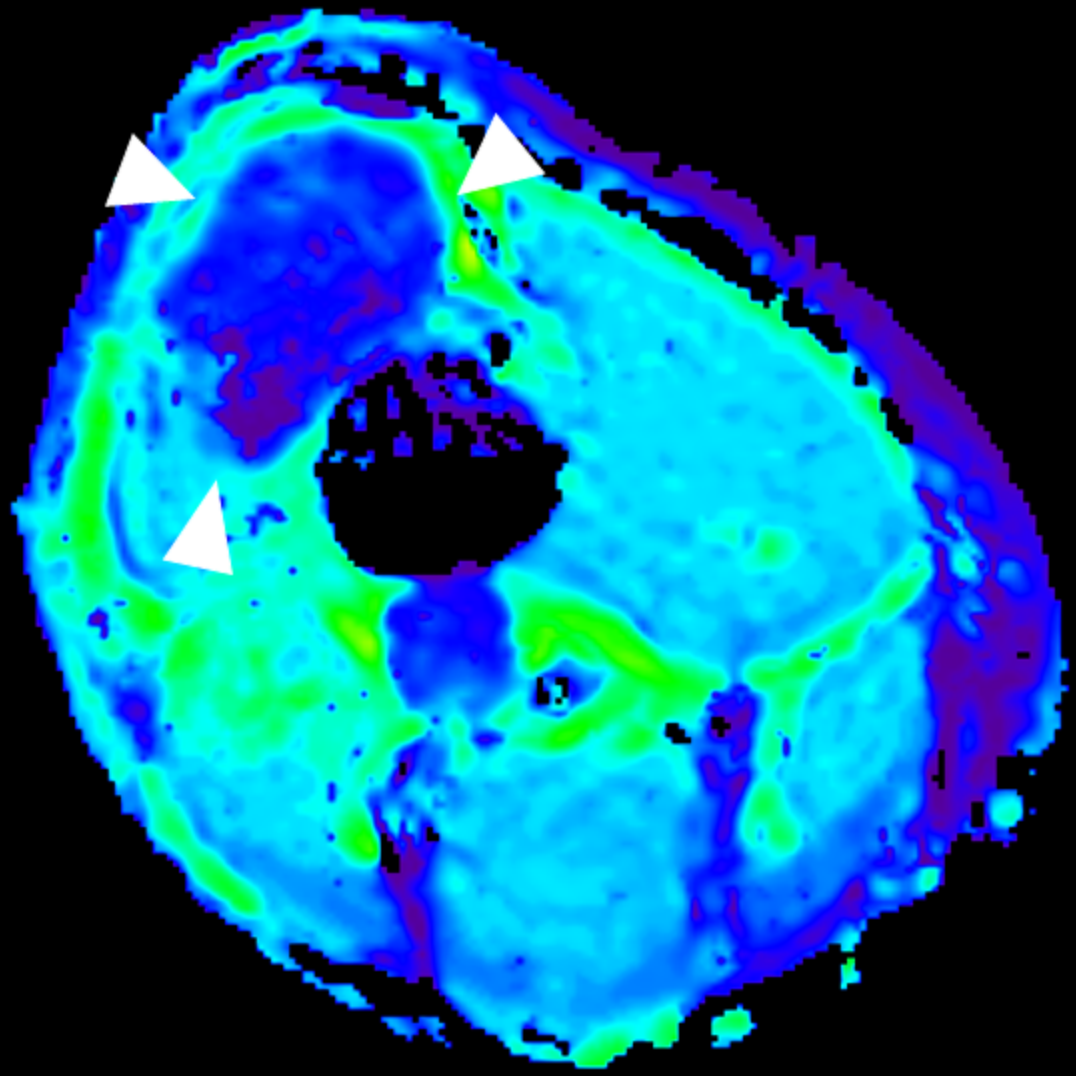

2

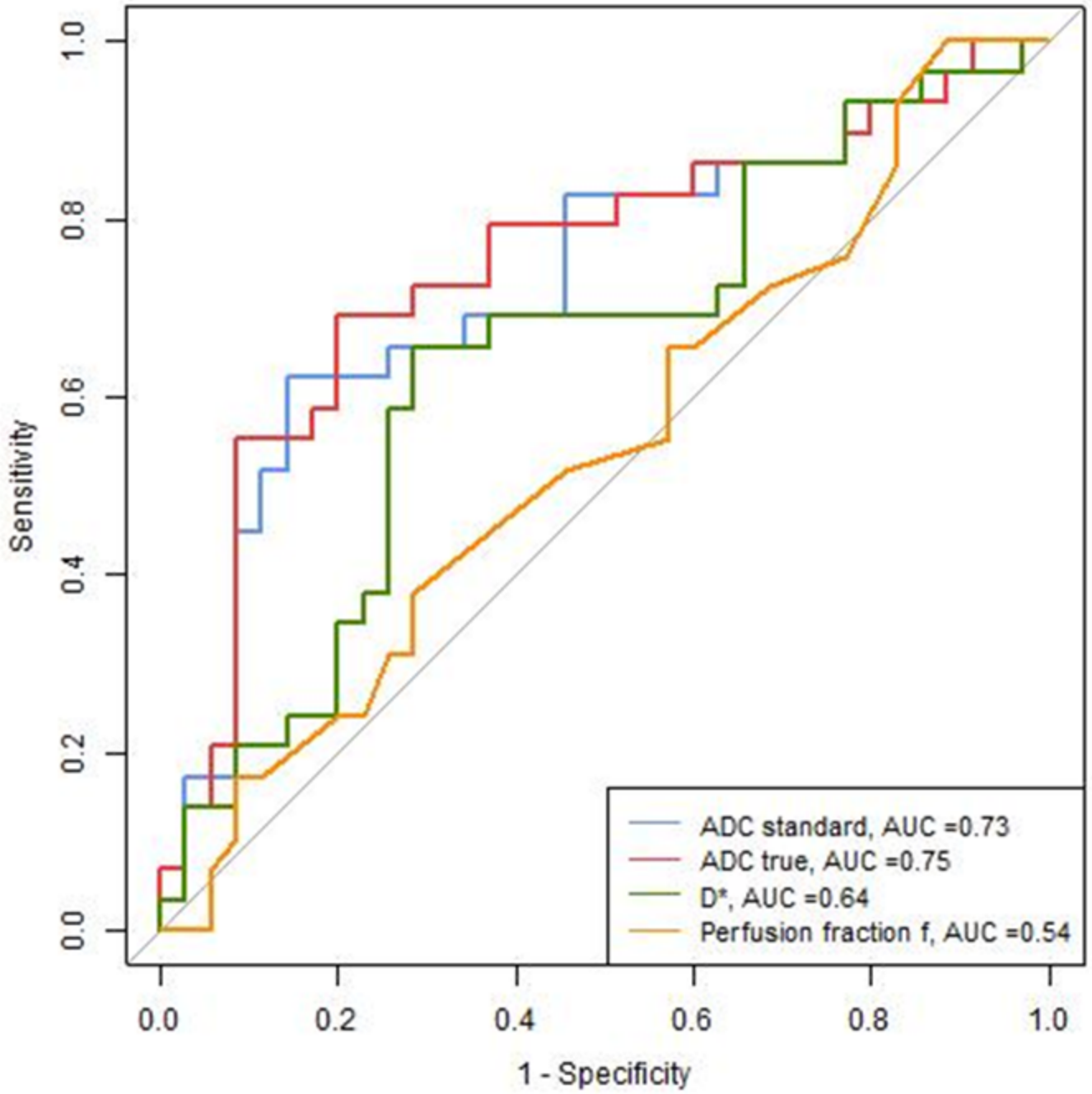


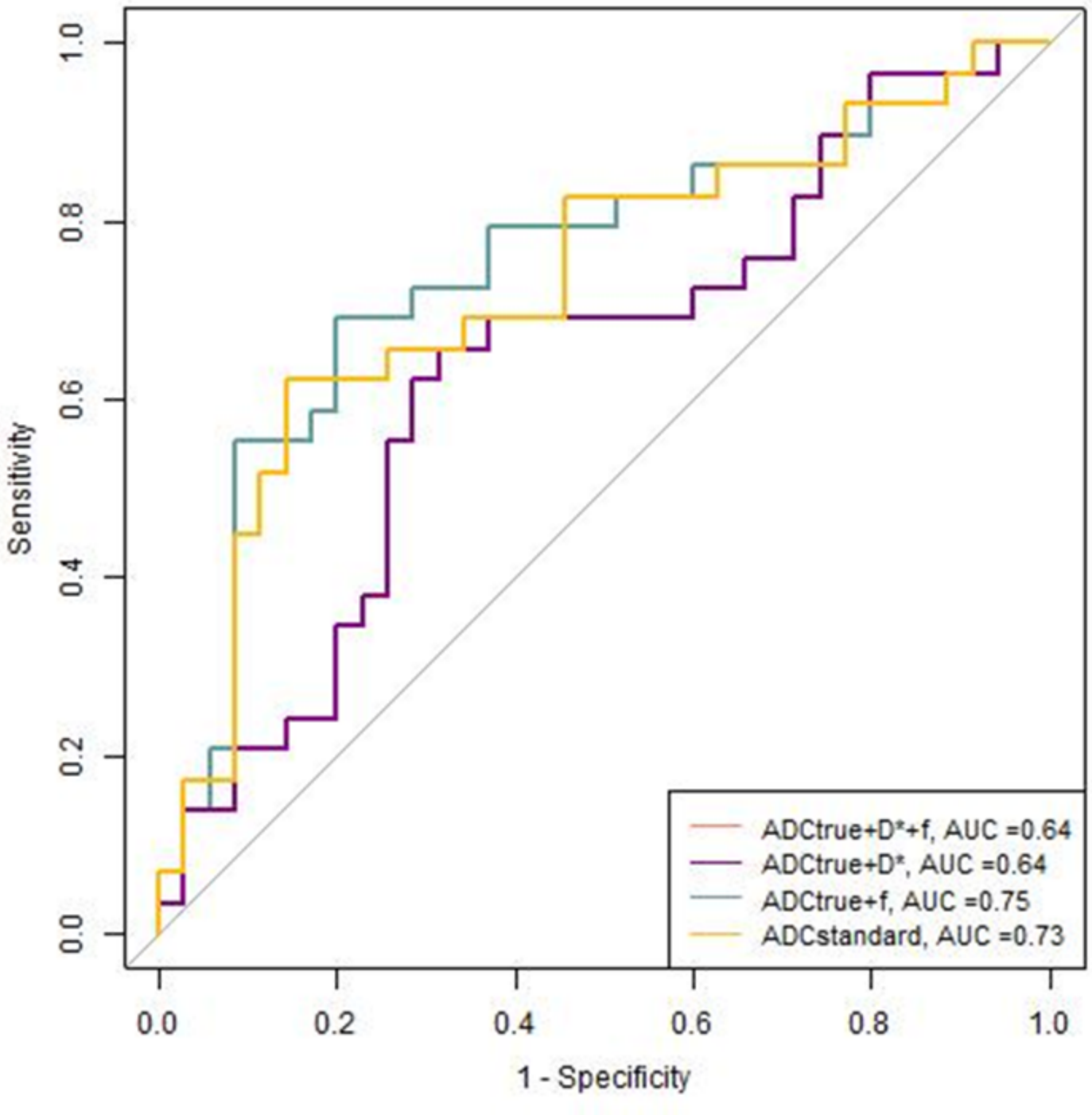

2

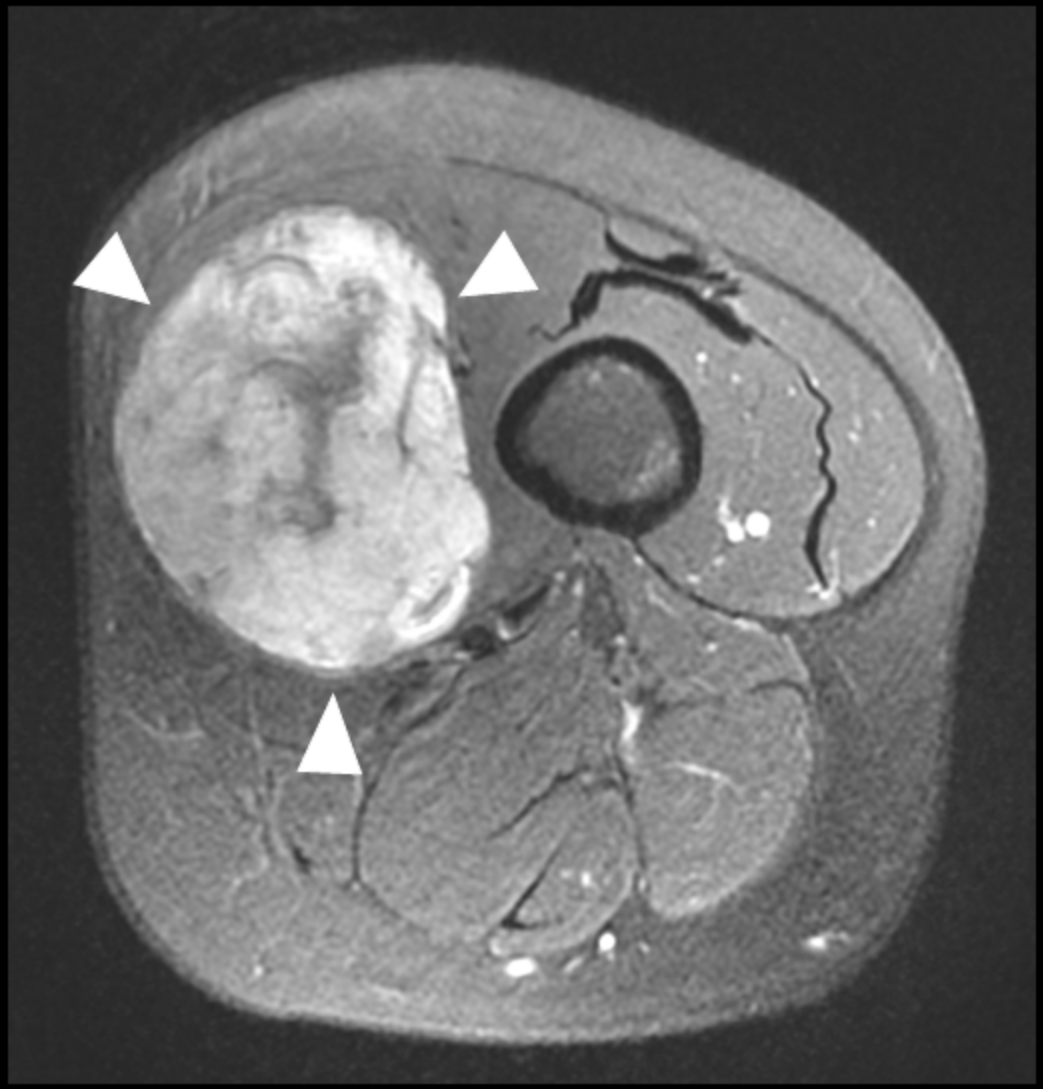

112

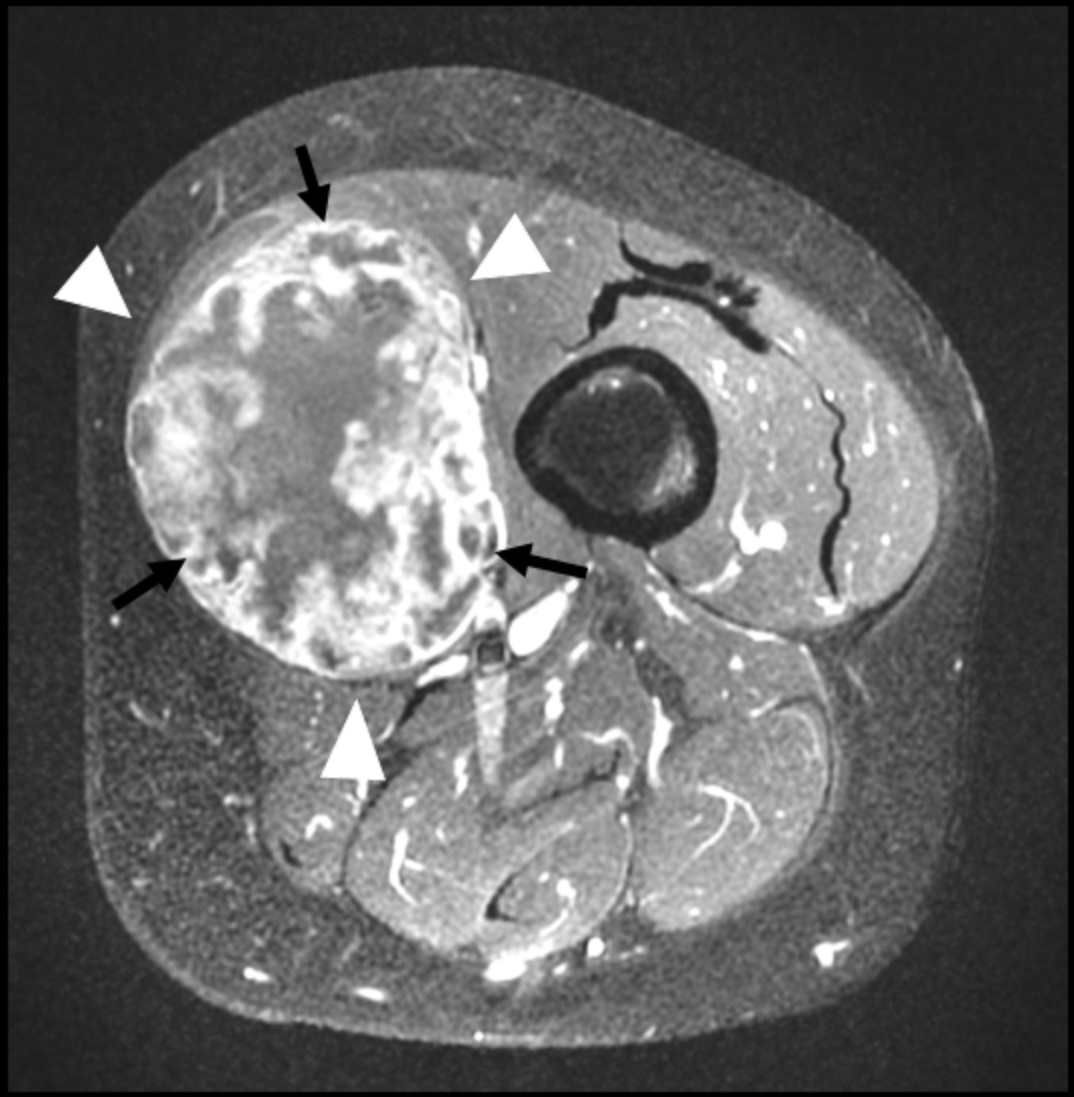


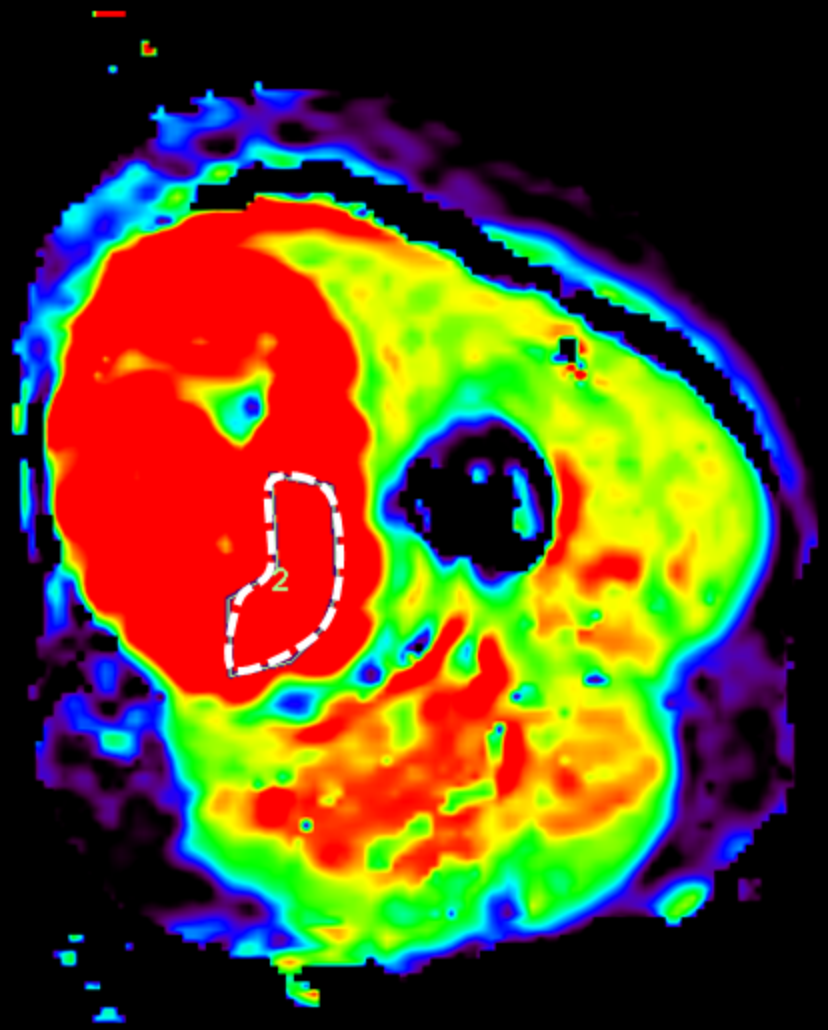


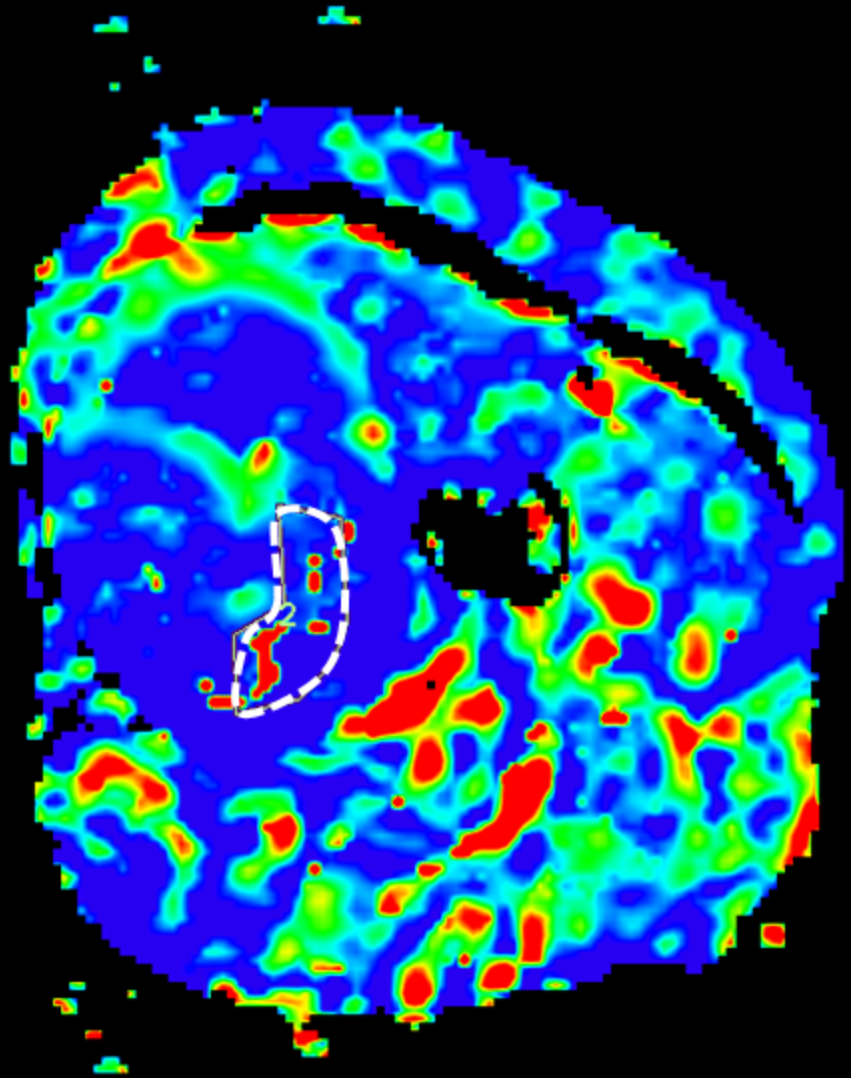

Sensitivity
1 - Specificity
0.0
0.2
0.4
0.6
0.8
1.0
ADC standard, AUC =0.73
ADC true, AUC =0.75
D*, AUC =0.64
Perfusion fraction f, AUC =0.54

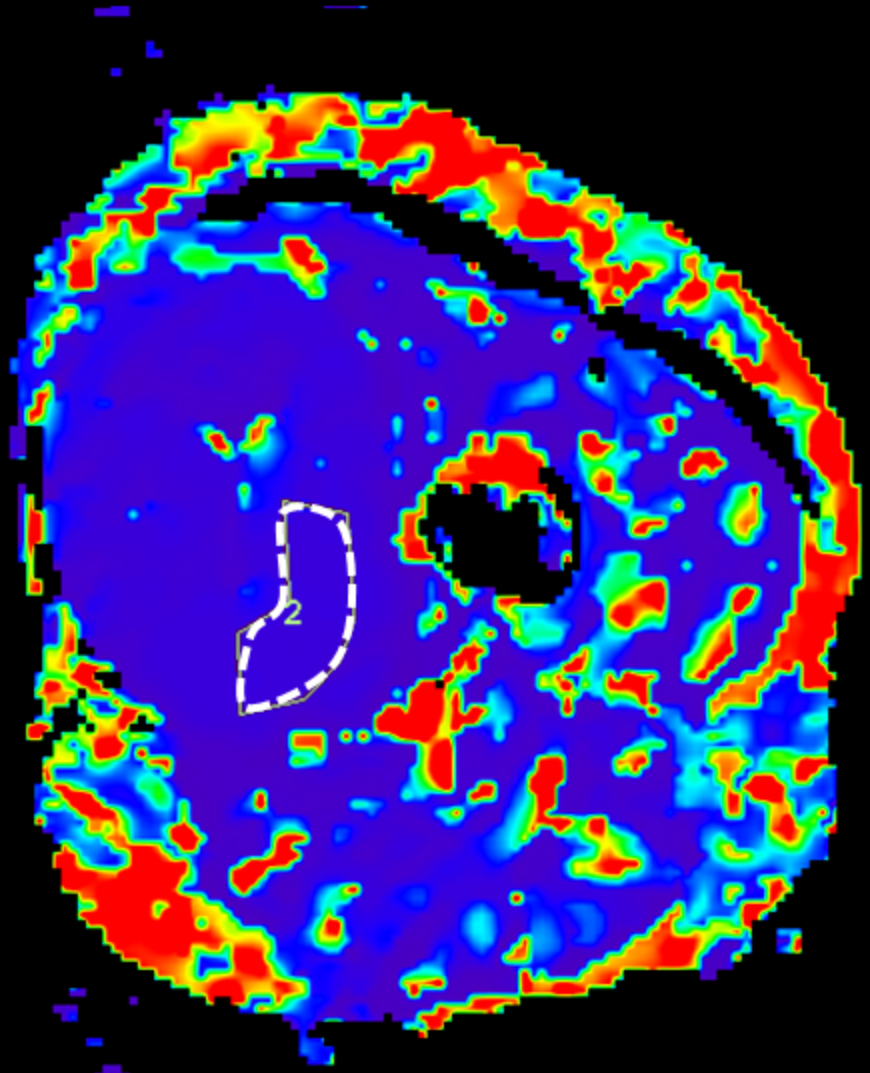

Sensitivity
1 - Specificity
0.0
0.2
0.4
0.6
0.8
1.0
ADCtrue+D*+f, AUC =0.64
ADCtrue+D*, AUC =0.64
ADCtrue+f, AUC =0.75
ADCstandard, AUC =0.73






2




2

Parameter*	T1-weighted	T2-weighted	CE T1-weighted	Diffusion weighted
Sequence type	FSE	FSE	FSE	SE-EPI
TE (ms)	7-19	39-111	8-13	< 80
TR (ms)	400-827	1718-8711	410-803	4000-17000**
B values (s/mm^2)	NA	NA	NA	20, 40, 60, 80, 100, 200, 300, 500, 700, 900
ETL	3	11-12	4	NA
Bandwidth (Khz)	25-35.7	27.7-31.2	31.25	166.7
NEX	0.5-2	1.5-5	0.5-3	1-4**
Acceleration factor	1.5-2.5	1.5-2.5	1.5-2.5	2
Fov (mm)	156×110 - 481×340	156×110 - 481×341	156×110 - 481×342	180×180 - 500×500
Matrix	128×128 - 512 × 448	128×128 - 512 × 449	128×128 - 512 × 450	96×128
Slice thickness (mm)	2.5 - 4	2.5 - 5	2.5 - 6	5
Gap (mm)	2.8 - 5	2.8 - 6	2.8 - 7	0.5
Fat-suppression	No	Yes	Yes	NA
Acquisition plane	1 orthogonal plane	2 orthogonal planes	1 orthogonal plane	Axial

* Parameter variations related to patient body habitus, coil and tumor size and location
** b value related variation
CE = Contrast enhanced; FSE = Fast spin echo; EPI = Echo planar imaging; NEX = Number of excitations; ETL = Echo train length; FOV = Field-of-view; NA = Not applicable

Benign tumors

Histologic subtype	Number of tumors	Percentage (%)
Schwannoma	13	20.3
Desmoid tumors	5	7.8
Myxomas	4	6.3
Neurofibromas	4	6.3
Giant cell tumors	3	4.7
Granular cell tumor	2	3.1
Myofibroblastic tumor	2	3.1
Leiomyoma	1	1.6
Solitary fibrous tumor	1	1.6

Malignant tumors

Histologic subtype	Number of tumors	Percentage (%)
Sarcoma*	24	37.5
B-cell lymphomas	2	3.1
Carcinomas	3	4.7

* Sarcoma subtypes are clear cell sarcoma, Ewing sarcoma, histiocytic sarcoma, fibromyxoid sarcoma, rhabdomyosarcoma, leiomyosarcoma, extraskeletal myxoid chondrosarcoma, sclerosing epithelioid fibrosarcoma and undifferentiated sarcoma.

Parameters	Reader	Benign tumors	Malignant tumors	*P* value	ICC
ADC_{true} ($*10^{-3}$ mm^2/s)	1	153.6 ± 50.9 [50.4-271.4]	112.9 ± 51.6 [46.7-240.4]	0.002	0.96
	2	153.5 ± 53.7 [44.8-274.4]	110 ± 49.9 [46.6-229.3]	0.001	
D* **($\times10^{-3}$ mm^2/s)**	1	841.5 ± 761.5 [150.5-3124.6]	1321.3 ± 1031.9 [211.7-4906.4]	0.05	0.91
	2	798.8 ± 794.3 [199.5-3003.6]	1450.7 ± 1061.1 [218-5199.7]	0.01	
f	1	0.1 ± 0.1 [0-0.2]	0.1 ± 0.1 [0-0.2]	0.58	0.81
	2	0.1 ± 0.1 [0-0.2]	0.1 ± 0 [0-0.3]	0.96	
ADC_{std} ($\times10^{-3}$ mm^2/s)	1	163.2 ± 51.4 [63.7-282.3]	123.7 ± 51.6 [52.1-249]	0.003	0.96
	2	163.2 ± 53.7 [59.3-290.1]	119.4 ± 50.4 [52.4-240.8]	0.001	

Values are presented as mean ± standard deviation; numbers in brackets are ranges.

ADC_{true} indicates the biexponential apparent diffusion coefficient; ADC_{std} indicates the monoexponential apparent diffusion coefficient; D* indicates tissue perfusion related coefficient and f indicates perfusion fraction. ICC indicates intraclass correlation coefficient.